**Sinteza** eISSN : 2797-8133
Jurnal Farmasi Klinis dan Sains Bahan Alam
Vol.6, No.1, Februari 2026, Hal. 37-51

# What Solvent is Actually the Best for Extracting Andrographolide? – Computational Evaluation of the Atomic Behavior in Different Solvent Models

**Arif Setiawansyah[1,2], Khairunnisa[3], Mayaranti Wilsya[3]**
[1]Pharmacy Diploma Program, Akademi Farmasi Cendikia Farma Husada, Bandar Lampung, Indonesia.
[2]Computational Research Center for Drug Discovery, PharmaSynthix Indonesia, Bandar Lampung, Indonesia
[3]Department of Pharmacy, STIK Siti Khadijah, Palembang, Indonesia
**Corresponding author: Arif Setiawansyah email: arif12.setiawansyah@gmail.com*

*Submitted:* 24-11-2025 *Revised:* 27-01-2026 *Accepted:* 29-01-2026
DOI: 10.29408/sinteza.v6i1.33127

**ABSTRACT**

Andrographolide, a bioactive diterpenoid lactone from *Andrographis paniculata*, exhibits significant anti-inflammatory, antimicrobial, and anticancer properties, making solvent selection critical for optimizing extraction efficiency while preserving bioactivity. This study aimed to identify the optimal solvent for andrographolide extraction through computational evaluation of solvation thermodynamics and electronic properties using density functional theory. Geometry optimization and solvation calculations were performed at the B3LYP/def2-SVP level using the Conductor-like Polarizable Continuum Model (CPCM) in ORCA version 6.0.1 across twelve solvent systems including water, alcohols, aprotic solvents, and non-polar media. Molecular properties including solvation free energy, frontier molecular orbitals, global chemical reactivity descriptors, dipole moment, atomic charge distribution, molecular electrostatic potential, and infrared spectra were systematically analyzed. Results demonstrated that water exhibited the most favorable solvation free energy at -76.64 kJ/mol, superior to all other examined solvents including acetonitrile (-75.30 kJ/mol), methanol (-75.05 kJ/mol), and significantly better than hexane (-33.52 kJ/mol). Water induces optimal dipole moment enhancement to 1.253 Debye while maintaining stable HOMO-LUMO energy gap of 5.009 eV and consistent global reactivity descriptors, confirming preservation of intrinsic chemical properties and bioactivity. Infrared spectroscopic analysis revealed complete structural integrity in aqueous environment. This computational study establishes water as the superior extraction medium for andrographolide based on exceptional thermodynamic favorability, optimal electronic stabilization, maintained molecular stability, and practical advantages including non-toxicity and environmental sustainability.

**Keywords: Andrographolide, Density Functional Theory, Solvation Free Energy, CPCM, Solvent Selection**

## INTRODUCTION

Andrographolide, a labdane diterpenoid lactone isolated from *Andrographis paniculata* (Burm.f.) Nees, has garnered substantial attention in pharmaceutical research due to its diverse biological activities, including anti-inflammatory (Low et al., 2024), antiviral (Adiguna et al., 2021), hepatoprotective (Mondal et al., 2022), and immunomodulatory properties (Iruretagoyena et al., 2005; Wang et al., 2010). The increasing demand for this bioactive compound in both traditional and modern medicine has necessitated the development of efficient extraction methodologies that can maximize yield while maintaining compound integrity. Solvent selection represents a critical parameter in the extraction process (Setiawansyah et al., 2025), as it directly influences not only the quantitative recovery of andrographolide but also the selectivity, cost-effectiveness, and environmental sustainability of the overall extraction procedure (Khosravanipour et al., 2021). Despite numerous experimental investigations into andrographolide extraction, the selection of optimal solvents has largely relied on empirical approaches and trial-and-error methodologies, which are time-consuming, resource-intensive, and often fail to provide comprehensive understanding of the underlying molecular mechanisms governing solute-solvent interactions (Luksta & Spalvins, 2023).

The efficiency of solvent extraction fundamentally depends on the thermodynamic favorability of solute dissolution, which is governed by intermolecular interactions between the target compound and solvent molecules (Mabesoone et al., 2020). Traditional experimental screening methods, while valuable, cannot fully elucidate the molecular-level phenomena such as hydrogen bonding patterns, dipole-dipole interactions, and van der Waals forces that determine solvation behavior. Furthermore, the extensive experimental testing required to evaluate multiple solvent systems generates significant chemical waste and incurs substantial operational costs (Khosravanipour et al., 2021). The emergence of computational chemistry, particularly *ab initio* quantum chemical methods, has opened new avenues for rational solvent design by enabling the prediction of molecular properties and interaction energies with high accuracy. These computational approaches can provide detailed insights into electronic structure, binding energies, and solvation free energies, thereby facilitating the identification of optimal solvents before committing resources to experimental validation (Da Silva et al., 2025; Sumer & Van Lehn, 2023).

Despite the growing application of computational methods in natural product chemistry, there remains a notable gap in the literature regarding systematic *ab initio* investigations of solvent effects on andrographolide extraction. While several studies have reported experimental solvent screening results (Cahyo et al., 2009; Rubi et al., 2019), nothing has attempted to correlate these findings with fundamental quantum chemical calculations that can explain the observed solubility trends. Previous computational studies on andrographolide compounds have primarily focused on conformational analysis or biological activity prediction (Zhang et al., 2024; Zuhriyah et al., 2025), leaving the crucial aspect of solvent selection largely unexplored from a first-principles perspective. This gap is particularly significant given that *ab initio* methods can account for subtle electronic effects and polarization phenomena that empirical or semi-empirical approaches may overlook, potentially leading to more accurate predictions of solvation behavior.

This investigation addresses the identified research gap by employing *ab initio* quantum mechanical calculations to systematically evaluate the interaction energies between andrographolide and a series of commonly used extraction solvents. The novelty of this work lies in its comprehensive computational framework that integrates electronic structure calculations with solvation models to predict optimal solvent systems based on fundamental molecular properties rather than purely empirical observations. By establishing quantitative structure-property relationships between solvent characteristics and extraction efficiency, this study provides a theoretical foundation for rational solvent selection that can significantly reduce the need for extensive experimental screening. The findings are expected to contribute not only to more efficient andrographolide extraction protocols but also to establish a broader computational methodology applicable to solvent optimization for other bioactive natural products, thereby advancing the field of green and sustainable extraction technologies.

## METHODS

### Materials and Instruments

This study utilized computational *in silico* methods employing a high-performance workstation operating on the Ubuntu system. The computational framework was equipped with an Intel® Core™ i9-12900KF processor containing 24 cores running at 3.2 GHz base frequency, 32 GB of random-access memory, and an NVIDIA RTX 4060 graphics card with 16 GB of dedicated video memory. The software suite integrated Avogadro, an open-source molecular editor and visualization tool, for constructing initial molecular structures and preparing input files, as well as for post-processing visualization of molecular geometries, orbital distributions, and electrostatic potential surfaces. ORCA version 6.0.1 served as the primary computational engine for performing quantum chemical simulations, including geometry optimizations, solvation calculations, frequency analyses, and electronic structure determinations.

**Structural optimization**

The geometry optimization of andrographolide was performed in the gas phase using ORCA version 6.0.1 at the B3LYP/def2-SVP level of theory with the def2/J auxiliary basis set (Neese, 2025). The optimization procedure employed standard gradient-based algorithms to locate the minimum energy structure on the potential energy surface. The calculation was initiated from an initial molecular geometry, and the optimization process iteratively adjusted atomic positions until convergence criteria were satisfied, including thresholds for energy change, maximum gradient, and root mean square gradient. The def2/J auxiliary basis set was utilized to accelerate the computation through the Resolution of Identity approximation for Coulomb integrals, significantly reducing computational cost while maintaining accuracy. Upon convergence (from Eh to kJ/mol), the optimized structure provided the equilibrium geometry with minimized total energy, which served as the reference structure for subsequent property calculations and solvation studies.

**Solvation simulation**

The solvation simulation of andrographolide was performed using the Conductor-like Polarizable Continuum Model (CPCM) to implicitly account for solvent effects (Stahn et al., 2023). The calculations were carried out at the B3LYP/def2-SVP level of theory with the def2/J auxiliary basis set for efficient computation of Coulomb integrals through the Resolution of Identity approximation. All calculations were carried out using ORCA version 6.0.1. Solvent effects were incorporated using the Conductor-like Polarizable Continuum Model (CPCM), in which the solute molecule was embedded in an implicit dielectric medium. A range of solvents with varying polarities was employed, including water, acetonitrile, acetone, ammonia, ethanol, methanol, dichloromethane ($CH_2Cl_2$), dimethylformamide (DMF), dimethyl sulfoxide (DMSO), ethyl acetate, chloroform, and hexane. Each solvent was defined by its corresponding dielectric constant within the CPCM framework. As an implicit solvation approach, CPCM does not require an explicit number or volume of solvent molecules; instead, the solvent environment is represented as a continuous polarizable medium surrounding the solute to evaluate solvation free energies and solvent-induced electronic effects.

**Data analysis**

The computational data analysis encompasses multiple molecular properties extracted from ORCA output files to characterize andrographolide comprehensively. The solvation free energy was calculated as the difference between total energies in solvent and gas phases to quantify dissolution favorability (equation 1) (He & Zhao, 2025).

$$Solvation\ free\ energy = Solvated\ free\ energy - Gas\ phase\ free\ energy \quad (1)$$

Global chemical reactivity descriptors including electron affinity, ionization, chemical hardness, softness, electronegativity, chemical potential, and electrophilicity index are derived from HOMO and LUMO energies using established theoretical equations (equation 2 – 8) (Siregar et al., 2026).

Electron affinity:

$A = - E_{LUMO}$ (2)

Electron ionization:

$I = - E_{HOMO}$ (3)

Chemical hardness:

$\eta = \frac{I-A}{2}$ (4)

Chemical softness:

$S = \frac{1}{2\eta}$ (5)

Electronegativity:

$\chi = \frac{I+A}{2}$ (6)

Chemical potential:

$\mu = -(\frac{I+A}{2})$ (7)

Electrophilicity index:

$\omega = \frac{\mu^2}{2\eta}$ (8)

Frontier molecular orbital analysis involves visualization of HOMO and LUMO distributions to identify reactive sites, while the HOMO-LUMO energy gap indicates kinetic stability (equation 9).

Energy gap:

$E\_gap = E_{LUMO} - E_{HOMO}$ (9)

The molecular electrostatic potential was mapped onto the electron density surface to reveal electrophilic and nucleophilic sites. Total dipole moment values were extracted to assess molecular polarity, and atomic charge distribution is analyzed using Mulliken population analysis to identify electron-rich and electron-deficient centers. The infrared spectrum was generated from frequency calculations at the optimized geometry, with characteristic vibrational bands assigned to specific functional groups for structural validation and comparison with experimental data.

## RESULTS AND DISCUSSION

### Structural optimization

The geometry optimization process reveals significant conformational rearrangement of andrographolide from its initial unoptimized structure to the final energy-minimized configuration. The unoptimized structure (Figure 1A), derived from standard chemical crystallographic coordinates retrieved from PubChem database, displays a relatively extended spatial arrangement with the lactone ring positioned at a considerable distance from the main decalin core. Upon optimization at the B3LYP/def2-SVP level in the gas phase, the molecule undergoes substantial structural relaxation, adopting a more compact and energetically favorable three-dimensional conformation. The optimized geometry demonstrates pronounced changes in the relative positioning of key structural elements, particularly the reorientation of the lactone moiety and the adjustment of hydroxyl group orientations (Wang & Song, 2016). These conformational changes reflect the molecule's tendency to minimize steric repulsion while maximizing stabilizing intramolecular interactions, potentially including weak hydrogen bonding between hydroxyl groups and carbonyl oxygen atoms. The decalin ring system maintains its characteristic chair-chair conformation in both structures, though subtle adjustments in ring puckering occur during optimization to achieve optimal bond angles and dihedral configurations (Sosnowska et al., 2025; Wang & Song, 2016).

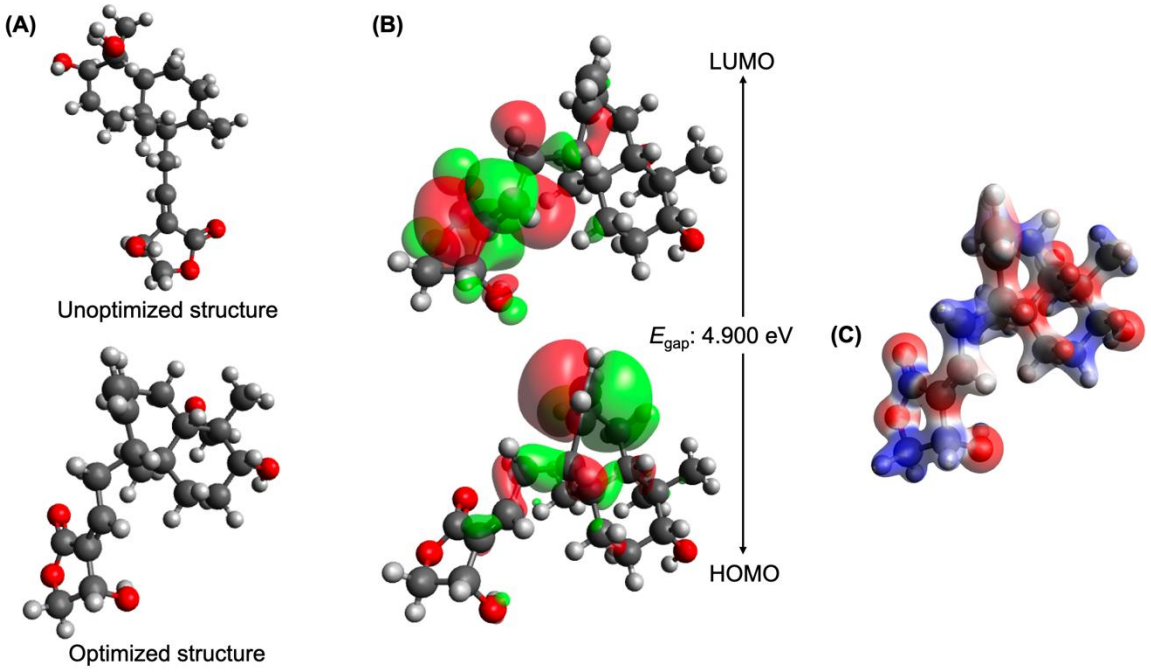


Figure 1. Structural and electronic properties of andrographolide from B3LYP/def2-SVP gas phase calculations. (A) Unoptimized (top) and optimized (bottom) molecular structures showing conformational changes during geometry optimization. (B) Frontier molecular orbitals (HOMO and LUMO), where red and green represent opposite orbital phases. (C) Molecular electrostatic potential map with color gradient from blue (positive potential) to red (negative potential), indicating reactive sites and hydrogen bonding regions.

The structural relaxation achieved through geometry optimization directly influences the electronic properties of andrographolide, as evidenced by the frontier molecular orbital analysis in Figure 1B. The highest occupied molecular orbital exhibits substantial electron density distribution across the conjugated lactone system and adjacent carbon framework, with notable contributions from the oxygen lone pairs. The orbital lobes display characteristic π-bonding character, with positive and negative phases indicated by red and green coloring respectively, demonstrating the delocalized nature of the highest energy electrons within the molecular framework (Isshiki et al., 2024; Maqbool & Ayub, 2024). The lowest unoccupied molecular orbital shows a distinctly different spatial distribution, with significant antibonding character concentrated in regions that would facilitate electron acceptance during nucleophilic attack or reduction processes. The calculated Highest Occupied Molecular Orbital-Lowest Unoccupied Molecular Orbital (HOMO-LUMO) energy gap of 4.900 eV in the gas phase indicates moderate kinetic stability, as this gap represents the minimum energy required for electronic excitation (Mohamed et al., 2025). This value suggests that andrographolide possesses sufficient electronic stability under standard laboratory isolation and handling conditions, which typically involve ambient temperature and common organic solvents, while maintaining adequate electronic accessibility to participate in biochemical interactions.

The spatial distribution of frontier orbitals provides essential context for understanding the molecular electrostatic potential map (Figure 1C), which reveals the three-dimensional distribution of electrostatic charge across the molecular surface. The color gradient from blue through white to red corresponds to the continuum from electron-deficient positive potential regions to electron-rich negative potential areas. The map demonstrates substantial negative potential concentrated around oxygen atoms, particularly those associated with hydroxyl groups and the lactone carbonyl, appearing as intense red

regions. These areas represent sites of high electron density that can serve as hydrogen bond acceptors or coordinate with electrophilic species. Conversely, regions of positive electrostatic potential, indicated by blue coloration, appear primarily around hydrogen atoms bonded to oxygen and carbon, identifying potential hydrogen bond donor sites and areas susceptible to nucleophilic attack (Domingo et al., 2024; Mata et al., 2010). The intermediate white and pink regions represent neutral or slightly polarized zones corresponding to the hydrocarbon framework.

This electrostatic potential distribution will directly correlate with the solvation behavior in subsequent CPCM calculations, as polar solvents capable of forming hydrogen bonds interact favorably with the pronounced electronegative regions around oxygen functionalities (Polonius et al., 2023; Souza et al., 2024). The spatial arrangement of positive and negative potential zones creates a complex electrostatic landscape that governs molecular recognition processes, explaining andrographolide's capacity to interact with biological macromolecules through complementary electrostatic interactions (Shashikala et al., 2019). The asymmetric distribution of electrostatic potential also contributes to the molecular dipole moment, with the concentration of negative potential on one molecular face and positive potential on the opposite side generating the observed dipole enhancement in polar solvents (Unke & Meuwly, 2019). The optimized structure therefore serves as the foundation for all subsequent property calculations, ensuring that computed molecular properties, including solvation energies, frontier orbital energies, and electrostatic potentials, correspond to the true energy minimum rather than an arbitrary starting geometry. This comprehensive characterization of the gas phase structure establishes the reference state against which solvent effects can be accurately assessed in the solvation energy calculations.

**Solvation thermodynamics and affinity**

The solvation free energy calculations provide fundamental insights into the thermodynamic favorability of andrographolide dissolution across various solvent systems. The data reveals (Figure 2) that all examined solvents exhibit negative solvation free energies, indicating spontaneous dissolution processes. However, the magnitude of these values varies significantly, ranging from -33.52 kJ/mol in hexane to -76.64 kJ/mol in water. The most polar protic solvents, particularly water (-76.64 kJ/mol), acetonitrile (-75.30 kJ/mol), and acetone (-73.50 kJ/mol), demonstrate the strongest solvation interactions with andrographolide. This observation suggests that the molecular architecture of andrographolide, which contains multiple hydroxyl groups and a lactone ring, establishes favorable hydrogen bonding networks and dipole-dipole interactions with polar solvent environments (Domingo et al., 2024; Unke & Meuwly, 2019). The intermediate polarity solvents such as methanol (-75.05 kJ/mol), ethanol (-74.23 kJ/mol), and dimethylsulfoxide (-75.87 kJ/mol) also exhibit substantial negative solvation energies, reflecting their capacity to accommodate both the hydrophilic and hydrophobic regions of the andrographolide structure.

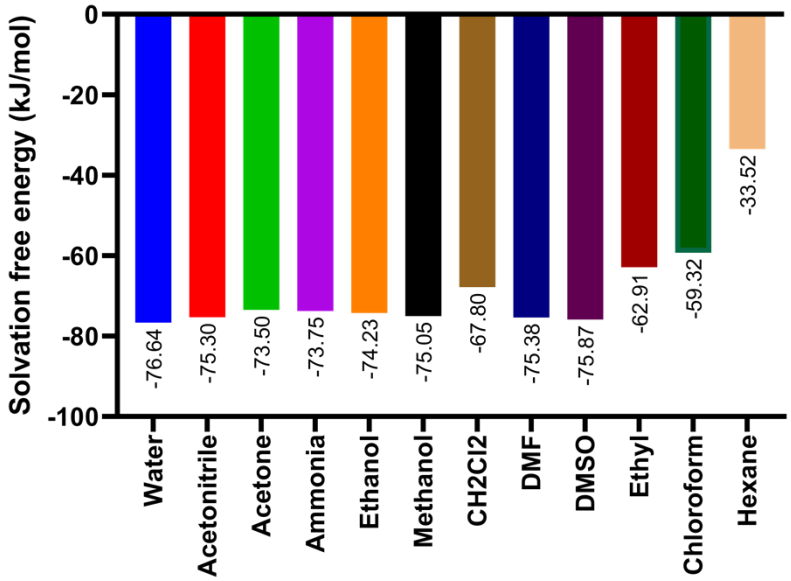


Figure 2. Solvation free energy of andrographolide in various solvent systems calculated at the B3LYP/def2-SVP level using the CPCM implicit solvation model.

The notably less negative solvation free energy observed in hexane (-33.52 kJ/mol) and chloroform (-59.32 kJ/mol) indicates weaker solute-solvent interactions in non-polar and weakly polar environments. This finding aligns with the limited capacity of these solvents to form hydrogen bonds with andrographolide's polar functional groups, resulting in thermodynamically less favorable dissolution (Zarić et al., 2020). The pronounced difference between polar and non-polar solvents underscores the critical role of polarity matching in optimizing extraction efficiency, where solvents capable of forming extensive intermolecular interactions with andrographolide exhibit more favorable solvation thermodynamics; however, this analysis is limited to idealized implicit solvation conditions and does not explicitly account for experimental variables such as temperature fluctuations, solvent mixtures, pH, or solid–matrix effects that may influence extraction behavior in real systems.

**Electronic distribution and solvent-induced polarization**

The atomic charge distribution analysis (Figure 3) reveals the influence of solvent polarity on the electronic structure of andrographolide, particularly at key functional sites. The data demonstrates that oxygen atoms, especially those associated with hydroxyl groups and the lactone carbonyl (atoms 21, 24, 27, and 26), carry substantial negative charges ranging from approximately -0.30 to -0.35 atomic units across most solvents. These electron-rich centers serve as primary sites for electrophilic interactions and hydrogen bond acceptance. Conversely, hydrogen atoms bonded to electronegative atoms exhibit positive charges, with hydroxyl hydrogens showing values near +0.20 to +0.25 atomic units, indicating their role as hydrogen bond donors.

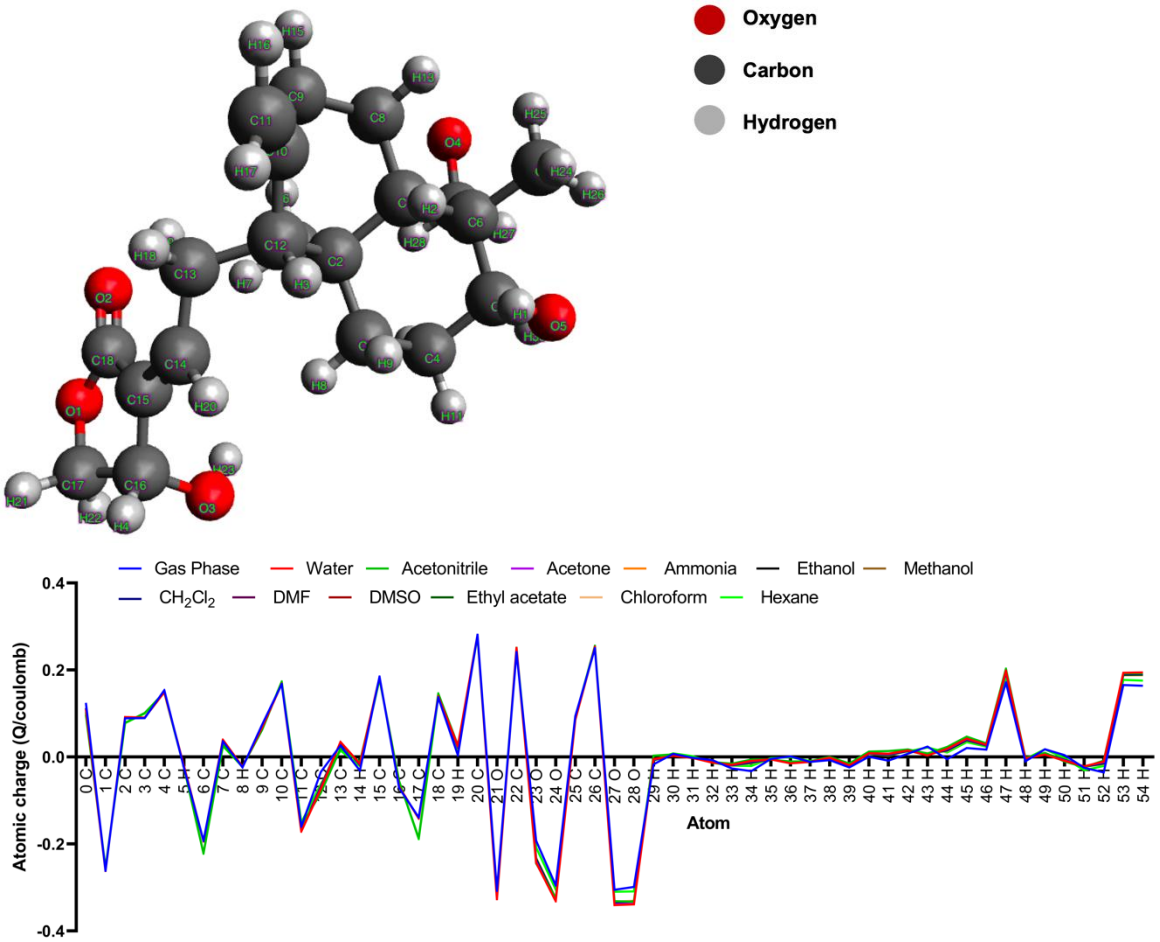


Figure 3. Atomic charge distribution of andrographolide across different atoms in gas phase and various solvent environments calculated using Mulliken population analysis at the B3LYP/def2-SVP level with CPCM.

The convergence of atomic charge patterns across different polar solvents suggests that once a threshold polarity is reached, the electronic redistribution within andrographolide approaches a limiting value. The gas phase calculation shows more pronounced charge localization compared to solvated states, as evidenced by the sharper peaks and troughs in the charge distribution profile. This observation indicates that polar solvents induce electronic polarization in andrographolide, moderating extreme charge densities through stabilizing electrostatic interactions (Gil et al., 2019; R. et al., 2023). The similar charge distribution patterns observed in water, acetonitrile, acetone, and alcoholic solvents reflect comparable polarization effects, which facilitate similar intermolecular interaction profiles and contribute to their uniformly favorable solvation energies.

**Vibrational spectroscopy and structural stability**

The infrared spectroscopic analysis (Figure 4) provides evidence for the structural integrity of andrographolide across different solvent environments. The overlapping IR spectra demonstrate that the fundamental vibrational modes remain largely invariant regardless of solvent polarity, with characteristic absorption bands appearing at consistent frequencies across all systems. The broad absorption region at 3838 $cm^{-1}$ corresponds to O-H stretching vibrations, while the sharp intense band at 1728 $cm^{-1}$ is attributed to the C=O stretching mode of the lactone group. Additional characteristic peaks at 1117 $cm^{-1}$ region represent C-O stretching and C-H bending vibrations.

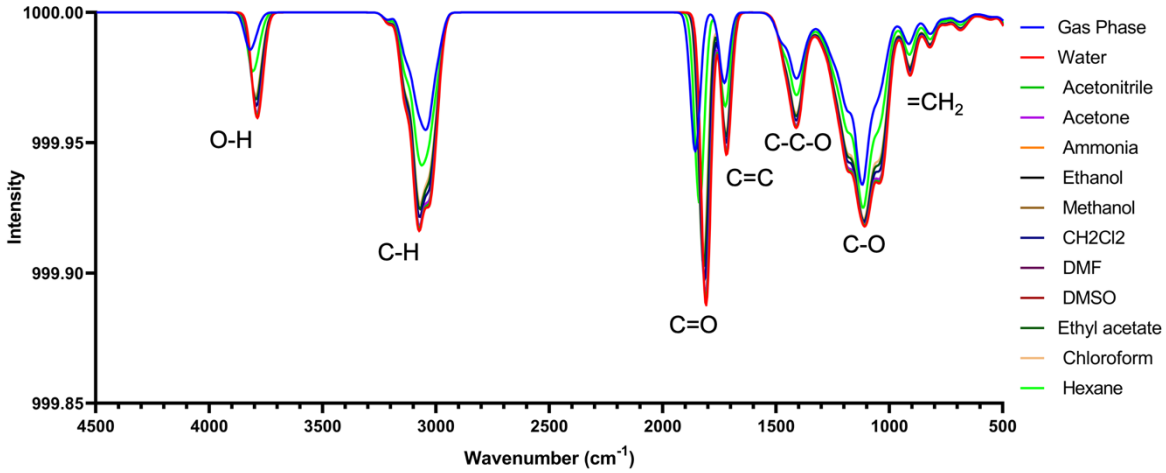


Figure 4. Theoretical infrared spectra of andrographolide in gas phase and various solvent environments calculated at the B3LYP/def2-SVP level of theory using the CPCM solvation model.

The remarkable similarity in spectral profiles indicates that solvent effects do not significantly alter the molecular geometry or intramolecular bonding characteristics of andrographolide. The minor spectral variations observed, particularly subtle frequency shifts in the hydroxyl and carbonyl regions, reflect weak intermolecular hydrogen bonding interactions with the solvent rather than fundamental structural changes (Banerjee & Chakraborty, 2018; Rakipov et al., 2022). This spectral consistency across diverse solvent polarities confirms that andrographolide maintains its molecular integrity during solvation, with the primary solvent influence manifesting as external stabilization rather than structural perturbation. Such stability is advantageous for extraction applications, as it ensures that the bioactive compound retains its native conformation regardless of the selected solvent system.

**Molecular polarity and dipole moment enhancement**

The total dipole moment analysis (Table 1) reveals significant solvent-induced polarization effects on the electronic distribution of andrographolide. The gas phase dipole moment of 0.90 Debye increases substantially upon solvation, with values ranging from 1.09 Debye in hexane to 1.27 Debye in DMSO and chloroform. This enhancement reflects the molecule's response to the external electric field generated by the surrounding solvent, where polar environments induce greater charge separation within andrographolide to minimize the overall system energy (Mahmood et al., 2022). The trend shows that more polar solvents generally produce larger dipole moments, with water (1.25 Debye), acetonitrile (1.24 Debye), and DMSO (1.27 Debye) inducing the most pronounced polarization.

The correlation between dipole moment enhancement and solvation free energy provides mechanistic insight into the dissolution process. Solvents that induce greater molecular polarization simultaneously achieve more favorable solvation energetics, as the enhanced dipole moment facilitates stronger electrostatic interactions with the solvent continuum (Giordano et al., 2025; Mélin et al., 2004). The relatively modest dipole moment increase in hexane (1.09 Debye) corresponds to its weak solvation capacity, while the substantial enhancement in polar aprotic solvents like DMSO reflects optimal electronic complementarity between solute and solvent. This relationship indicates that the extraction efficiency of andrographolide depends not only on solvent polarity but also on the solvent's ability to induce favorable electronic reorganization in the solute molecule.

**Table 1.** Total dipole moment components of andrographolide in gas phase and various solvent environments calculated at the B3LYP/def2-SVP level using CPCM.

| Solvents | Total dipole moment | | |
|---|---|---|---|
| | μX | μY | μZ |
| Water | 1.253420040 | 0.620702751 | -0.675523021 |
| Acetonitrile | 1.238691486 | 0.617213972 | -0.664678277 |
| Acetone | 1.221520329 | 0.609444429 | -0.655116720 |
| Ammonia | 1.224025471 | 0.610385515 | -0.656564978 |
| Ethanol | 1.228628911 | 0.612592067 | -0.659219198 |
| Methanol | 1.236489274 | 0.615920587 | -0.663519093 |
| CH2Cl2 | 1.167932229 | 0.591734696 | -0.623426427 |
| DMF | 1.239534758 | 0.617529110 | -0.665166586 |
| DMSO | 1.245821666 | 0.617168446 | -0.671149460 |
| Ethyl acetate | 1.126358360 | 0.571861769 | -0.603525157 |
| Chloroform | 1.096378707 | 0.564185953 | -0.585411326 |
| Hexane | 0.904226706 | 0.488435927 | -0.483700845 |

**Chemical reactivity and frontier orbital analysis**

The global chemical reactivity descriptors (Table 2) derived from frontier molecular orbital energies provide comprehensive characterization of andrographolide's electronic properties across different environments. The HOMO energies remain relatively stable around -6.50 eV across most solvents, while LUMO energies cluster near -1.50 eV, resulting in HOMO-LUMO energy gaps ranging from 4.90 eV in the gas phase to approximately 5.01 eV in polar solvents. This moderate energy gap indicates reasonable kinetic stability while maintaining sufficient electronic accessibility for biological and solvent interactions. The water solvated phase exhibits the largest energy gap (5.011 eV), suggesting enhanced stability in the presence of water molecule, whereas other solvated states show slightly reduced gaps reflecting modest destabilization of frontier orbitals through solvent-orbital interactions.

The ionization potential values, derived from negative HOMO energies, range from 6.509 to 6.559 eV, indicating that andrographolide exhibits moderate resistance to electron loss across all solvent environments. The electron affinity values, calculated from negative LUMO energies, vary from 1.500 to 1.659 eV, suggesting modest electron-accepting capability. The chemical hardness parameter, which quantifies resistance to electronic perturbation, ranges from 2.474 to 2.506 eV in solvated states compared to 2.450 eV in gas phase, demonstrating that solvent effects minimally impact the intrinsic electronic robustness of the molecule. Conversely, chemical softness values of approximately 0.20 $eV^{-1}$ indicate moderate polarizability and responsiveness to external perturbations.

The electronegativity values, averaging around 4.00 eV across all solvents, reflect andrographolide's balanced electronic character without extreme electron-withdrawing or electron-donating tendencies. The chemical potential, representing the molecule's tendency to lose electrons, remains consistently negative at approximately -4.00 eV across environments, indicating thermodynamic favorability for electron retention. The electrophilicity index, which quantifies the molecule's capacity to accept electrons from electron-rich environments, varies from 3.199 to 3.446, with the gas phase exhibiting the highest value (3.446). This moderate electrophilicity suggests that andrographolide can participate in nucleophilic interactions, which may contribute to its biological activity through interactions with electron-rich biomolecular targets.

Table 2. Global chemical reactivity descriptors of andrographolide derived from frontier molecular orbital energies calculated at the B3LYP/def2-SVP level using CPCM. Parameters include ionization potential (I), electron affinity (A), HOMO-LUMO energy gap (E_gap), chemical hardness (η), chemical softness (S), electronegativity (χ), chemical potential (μ), and electrophilicity index (ω).

| Solvent | Energy (eV) | | | | | | | | | |
|---|---|---|---|---|---|---|---|---|---|---|
| | **HOMO** | **LUMO** | **E_gap** | ***I*** | ***A*** | ***η*** | ***S*** | ***χ*** | ***μ*** | ***ω*** |
| Water | -6.509 | -1.498 | 5.011 | 6.509 | 1.498 | 2.506 | 0.200 | 4.004 | -4.004 | 3.199 |
| Acetonitrile | -6.509 | -1.500 | 5.009 | 6.509 | 1.500 | 2.505 | 0.200 | 4.005 | -4.005 | 3.201 |
| Acetone | -6.510 | -1.504 | 5.006 | 6.510 | 1.504 | 2.503 | 0.200 | 4.007 | -4.007 | 3.207 |
| Ammonia | -6.510 | -1.503 | 5.007 | 6.510 | 1.503 | 2.504 | 0.200 | 4.007 | -4.007 | 3.206 |
| Ethanol | -6.510 | -1.502 | 5.008 | 6.510 | 1.502 | 2.504 | 0.200 | 4.006 | -4.006 | 3.204 |
| Methanol | -6.509 | -1.501 | 5.008 | 6.509 | 1.501 | 2.504 | 0.200 | 4.005 | -4.005 | 3.203 |
| $CH_2Cl_2$ | -6.512 | -1.514 | 4.998 | 6.512 | 1.514 | 2.499 | 0.200 | 4.013 | -4.013 | 3.222 |
| DMF | -6.509 | -1.500 | 5.009 | 6.509 | 1.500 | 2.505 | 0.200 | 4.005 | -4.005 | 3.201 |
| DMSO | -6.509 | -1.499 | 5.010 | 6.509 | 1.499 | 2.505 | 0.200 | 4.004 | -4.004 | 3.200 |
| Ethyl acetate | -6.514 | -1.523 | 4.991 | 6.514 | 1.523 | 2.496 | 0.200 | 4.019 | -4.019 | 3.235 |
| Chloroform | -6.516 | -1.530 | 4.986 | 6.516 | 1.530 | 2.493 | 0.201 | 4.023 | -4.023 | 3.246 |
| Hexane | -6.532 | -1.584 | 4.948 | 6.532 | 1.584 | 2.474 | 0.202 | 4.058 | -4.058 | 3.328 |
| Gas Phase | -6.559 | -1.659 | 4.900 | 6.559 | 1.659 | 2.450 | 0.204 | 4.109 | -4.109 | 3.446 |

**Integrated Solvent Selection Strategy**

The comprehensive analysis of thermodynamic, electronic, spectroscopic, and reactivity parameters establishes a rational framework for solvent selection in andrographolide extraction. The convergence of multiple analytical dimensions reveals that polar protic solvents, particularly water, methanol, and ethanol, along with polar aprotic solvents such as acetonitrile and DMSO, provide optimal solvation environments. These solvents demonstrate the most negative solvation free energies, induce substantial dipole moment enhancement, and maintain consistent molecular structure as evidenced by IR spectroscopy. The global reactivity descriptors remain relatively invariant across these solvents, indicating that extraction conditions can be optimized based primarily on solvation thermodynamics without compromising the electronic integrity or bioactivity of andrographolide.

From a practical extraction perspective, the computational analysis unequivocally establishes water as the optimal extraction medium for andrographolide based on its superior thermodynamic performance. Water demonstrates the most negative solvation free energy, surpassing all other examined solvents and indicating the strongest spontaneous

dissolution capacity. This exceptional solvation performance is attributed to water's unique ability to form extensive and stable hydrogen bonding networks with the multiple hydroxyl groups and lactone functionality of andrographolide, maximizing solute-solvent interactions and extraction efficiency. Beyond its thermodynamic superiority, water offers compelling practical advantages that reinforce its selection as the preferred extraction solvent. The non-toxic nature of water ensures operator safety and eliminates concerns regarding hazardous chemical exposure during large-scale extraction operations. The environmental sustainability of water-based extraction processes aligns with green chemistry principles, eliminating the generation of organic solvent waste that requires costly disposal and poses environmental risks (Khosravanipour et al., 2021).

In contrast, the computational data clearly indicates that hexane and other non-polar solvents must be avoided due to significantly less favorable solvation energetics, which would result in substantially lower extraction yields. While other polar solvents such as acetonitrile and methanol demonstrate favorable solvation properties, none surpass water's performance. The moderate electrophilicity and balanced chemical reactivity descriptors of andrographolide in aqueous solution confirm that the compound maintains its characteristic electronic properties and bioactive potential during water-based extraction, ensuring that the isolated compound retains full pharmaceutical efficacy for subsequent applications.

## CONCLUSION

The CPCM-based solvation analysis at the B3LYP/def2-SVP level indicates that water provides the most thermodynamically favorable solvation for andrographolide among the investigated solvents, as reflected by the most negative solvation free energy (−76.64 kJ/mol). This enhanced solvation is attributed to strong hydrogen-bonding interactions between water and the hydroxyl and lactone groups of andrographolide, while preserving molecular stability as evidenced by a maintained HOMO–LUMO energy gap and stable electronic descriptors. However, these findings are derived from an implicit solvation model under idealized conditions and do not explicitly consider experimental variables such as temperature, solvent mixtures, pH, or solid–matrix interactions, which may influence extraction performance in practical applications.

## ACKNOWLEDGEMENT

None to declare.

## REFERENCES

Adiguna, S. P., Panggabean, J. A., Atikana, A., Untari, F., Izzati, F., Bayu, A., Rosyidah, A., Rahmawati, S. I., & Putra, M. Y. (2021). Antiviral Activities of Andrographolide and Its Derivatives: Mechanism of Action and Delivery System. *Pharmaceuticals*, *14*(11), 1102. https://doi.org/10.3390/ph14111102

Banerjee, P., & Chakraborty, T. (2018). Weak hydrogen bonds: insights from vibrational spectroscopic studies. *International Reviews in Physical Chemistry*, *37*(1), 83–123. https://doi.org/10.1080/0144235X.2018.1419731

Cahyo Kumoro, A., Hasan, M., & Singh, H. (2009). Effects of Solvent Properties on the Soxhlet Extraction of Diterpenoid Lactones from Andrographis Paniculata Leaves. *ScienceAsia*, *35*(3), 306. https://doi.org/10.2306/scienceasia1513-1874.2009.35.306

Da Silva, H. C., Hernandes, I. S., & De Almeida, W. B. (2025). Modeling Solvent Effects in Quantum Chemical Calculation of Relative Energies and NMR Chemical Shifts for Azithromycin. *The Journal of Physical Chemistry A*, *129*(9), 2200–2216. https://doi.org/10.1021/acs.jpca.4c08015

Domingo, L. R., Pérez, P., Ríos-Gutiérrez, M., & Aurell, M. J. (2024). A molecular electron density theory study of hydrogen bond catalysed polar Diels–Alder reactions of α,β-

unsaturated carbonyl compounds. *Tetrahedron Chem*, *10*, 100064. https://doi.org/10.1016/j.tchem.2024.100064

Gil, G., Pipolo, S., Delgado, A., Rozzi, C. A., & Corni, S. (2019). Nonequilibrium Solvent Polarization Effects in Real-Time Electronic Dynamics of Solute Molecules Subject to Time-Dependent Electric Fields: A New Feature of the Polarizable Continuum Model. *Journal of Chemical Theory and Computation*, *15*(4), 2306–2319. https://doi.org/10.1021/acs.jctc.9b00010

Giordano, M., Alfano, F. O., Di Maio, F. P., & Di Renzo, A. (2025). Effective dipole model for electrostatic interactions between polarizable spherical particles in particle scale simulations. *Scientific Reports*, *15*(1), 3121. https://doi.org/10.1038/s41598-025-86181-x

He, Q., & Zhao, H. (2025). Pentoxifylline in sixteen pure solvents: Solubility, DFT calculation, and molecular dynamic simulation. *Journal of Molecular Liquids*, 429, 127610. https://doi.org/10.1016/j.molliq.2025.127610

Iruretagoyena, M. I., Tobar, J. A., González, P. A., Sepúlveda, S. E., Figueroa, C. A., Burgos, R. A., Hancke, J. L., & Kalergis, A. M. (2005). Andrographolide Interferes with T Cell Activation and Reduces Experimental Autoimmune Encephalomyelitis in the Mouse. *The Journal of Pharmacology and Experimental Therapeutics*, *312*(1), 366–372. https://doi.org/10.1124/jpet.104.072512

Isshiki, Y., Montes, E., Nishino, T., Vázquez, H., & Fujii, S. (2024). Resolving molecular frontier orbitals in molecular junctions with kHz resolution. *Chemical Science*, *15*(42), 17328–17336. https://doi.org/10.1039/D4SC05285D

Khosravanipour Mostafazadeh, A., Karimiestahbanati, M., Diop, A., Adjallé, K., Drogui, P., & Tyagi, R. D. (2021). Green Chemistry for Green Solvent Production and Sustainability Toward Green Economy. In *Biomass, Biofuels, Biochemicals* (pp. 583–636). Elsevier. https://doi.org/10.1016/B978-0-12-821878-5.00017-9

Low, M., Suresh, H., Zhou, X., Bhuyan, D. J., Alsherbiny, M. A., Khoo, C., Münch, G., & Li, C. G. (2024). The wide spectrum anti-inflammatory activity of andrographolide in comparison to NSAIDs: A promising therapeutic compound against the cytokine storm. *PLOS ONE*, *19*(7), e0299965. https://doi.org/10.1371/journal.pone.0299965

Luksta, I., & Spalvins, K. (2023). Methods for Extraction of Bioactive Compounds from Products: A Review. *Environmental and Climate Technologies*, *27*(1), 422–437. https://doi.org/10.2478/rtuect-2023-0031

Mabesoone, M. F. J., Palmans, A. R. A., & Meijer, E. W. (2020). Solute–Solvent Interactions in Modern Physical Organic Chemistry: Supramolecular Polymers as a Muse. *Journal of the American Chemical Society*, *142*(47), 19781–19798. https://doi.org/10.1021/jacs.0c09293

Mahmood, E. A., Poor Heravi, M. R., Khanmohammadi, A., Mohammadi-Aghdam, S., Ebadi, A. G., & Habibzadeh, S. (2022). DFT calculations, structural analysis, solvent effects, and non-covalent interaction study on the para-aminosalicylic acid complex as a tuberculosis drug: AIM, NBO, and NMR analyses. *Journal of Molecular Modeling*, *28*(10), 297. https://doi.org/10.1007/s00894-022-05279-5

Maqbool, M., & Ayub, K. (2024). Controlled tuning of HOMO and LUMO levels in supramolecular nano-Saturn complexes. *RSC Advances*, *14*(53), 39395–39407. https://doi.org/10.1039/D4RA07068B

Mata, I., Alkorta, I., Molins, E., & Espinosa, E. (2010). Universal Features of the Electron Density Distribution in Hydrogen-Bonding Regions: A Comprehensive Study

Involving H···X (X=H, C, N, O, F, S, Cl, π) Interactions. *Chemistry – A European Journal*, *16*(8), 2442–2452. https://doi.org/10.1002/chem.200901628

Mélin, T., Diesinger, H., Deresmes, D., & Stiévenard, D. (2004). Probing Nanoscale Dipole-Dipole Interactions by Electric Force Microscopy. *Physical Review Letters*, *92*(16), 166101. https://doi.org/10.1103/PhysRevLett.92.166101

Mohamed, A., Visco, D. P. Jr., Breimaier, K., & Bastidas, D. M. (2025). Effect of Molecular Structure on the B3LYP-Computed HOMO–LUMO Gap: A Structure −Property Relationship Using Atomic Signatures. *ACS Omega*, *10*(3), 2799–2808. https://doi.org/10.1021/acsomega.4c08626

Mondal, M., Sarkar, C., Saha, S., Hossain, M. N., Norouzi, R., Mubarak, M. S., Siyadatpanah, A., Wilairatana, P., Hossain, R., Islam, M. T., & Coutinho, H. D. M. (2022). Hepatoprotective activity of andrographolide possibly through antioxidative defense mechanism in Sprague-Dawley rats. *Toxicology Reports*, *9*, 1013–1022. https://doi.org/10.1016/j.toxrep.2022.04.007

Neese, F. (2025). Software Update: The ORCA Program System—Version 6.0. In *Wiley Interdisciplinary Reviews: Computational Molecular Science* (Vol. 15, Issue 2). John Wiley and Sons Inc. https://doi.org/10.1002/wcms.70019

Polonius, S., Zhuravel, O., Bachmair, B., & Mai, S. (2023). LVC/MM: A Hybrid Linear Vibronic Coupling/Molecular Mechanics Model with Distributed Multipole-Based Electrostatic Embedding for Highly Efficient Surface Hopping Dynamics in Solution. *Journal of Chemical Theory and Computation*, *19*(20), 7171–7186. https://doi.org/10.1021/acs.jctc.3c00805

R., A., Hu, J., & Momeen, M. U. (2023). Role of the solvent polarity on the optical and electronic characteristics of 1-iodoadamantane. *RSC Advances*, *13*(42), 29489–29495. https://doi.org/10.1039/D3RA05297D

Rakipov, I. T., Petrov, A. A., Akhmadiyarov, A. A., Khachatrian, A. A., & Varfolomeev, M. A. (2022). FTIR spectral study of intermolecular interactions of C=O groups of amides in solution. *Journal of Molecular Liquids*, *354*, 118838. https://doi.org/10.1016/j.molliq.2022.118838

Rubi, R. V. C., Quitain, A. T., Agutaya, J. K. C. N., Doma, B. T., Soriano, A. N., Auresenia, J., & Kida, T. (2019). Synergy of in-situ formation of carbonic acid and supercritical CO2-expanded liquids: Application to extraction of andrographolide from Andrographis paniculata. *The Journal of Supercritical Fluids*, *152*, 104546. https://doi.org/10.1016/j.supflu.2019.104546

Setiawansyah, A., Fiolita, B., Agatha, S., Sitindaon, R. S. E., Reynaldi, M. A., Hidayat, L. H., Hadi, I., Permatasari, L., Hidayati, N., Arsul, M. I., & Dirgantara, S. (2025). Impact of post-harvest process and methanol polarity on the content of niazirin, flavonoids, phenols, and antioxidant activity index of Moringa oleifera Lam leaves. *Food and Humanity*, *5*, 100767. https://doi.org/https://doi.org/10.1016/j.foohum.2025.100767

Shashikala, H. B. M., Chakravorty, A., & Alexov, E. (2019). Modeling Electrostatic Force in Protein-Protein Recognition. *Frontiers in Molecular Biosciences*, *6*. https://doi.org/10.3389/fmolb.2019.00094

Siregar, M. H., Nurdiana, N., Bal'afif, F., Djajalaksana, S., & Setiawansyah, A. (2026). Comprehensive Bioinformatics, Molecular Docking, and In Vivo Investigation of a Novel Mechanistic Pathway in Pentylenetetrazole-Induced Seizures. *Advanced Journal of Chemistry, Section A*, 9(5), 919–939. https://doi.org/10.48309/ajca.2026.561381.1974

Sosnowska, A., Chojnacki, J., Samaszko-Fiertek, J., Madaj, J., & Dmochowska, B. (2025). Crystal Structures of d-Lyxono-1,4-lactone and Its O-Tosyl Derivative. *Molecules*, *30*(2), 287. https://doi.org/10.3390/molecules30020287

Souza Junior, M. V., Oliveira Neto, J. G., Pereira, W. O., Rodrigues, J. A. O., Viana, J. R., Reis, A. S., Lage, M. R., Carvalho, G. G. C., Pessoa, C. O., Santos, A. O. dos, & Sousa, F. F. de. (2024). Comprehensive analysis of the electronic, thermodynamic, and spectroscopic properties of a Cu(II)-based complex with 1,10-phenanthroline and L-glutamine. *Heliyon*, *10*(20), e37505. https://doi.org/10.1016/j.heliyon.2024.e37505

Stahn, M., Ehlert, S., & Grimme, S. (2023). Extended Conductor-like Polarizable Continuum Solvation Model (CPCM-X) for Semiempirical Methods. *The Journal of Physical Chemistry A*, *127*(33), 7036–7043. https://doi.org/10.1021/acs.jpca.3c04382

Sumer, Z., & Van Lehn, R. C. (2023). Heuristic Computational Model for Predicting Lignin Solubility in Tailored Organic Solvents. *ACS Sustainable Chemistry & Engineering*, *11*(1), 187–198. https://doi.org/10.1021/acssuschemeng.2c05199

Unke, O. T., & Meuwly, M. (2019). PhysNet: A Neural Network for Predicting Energies, Forces, Dipole Moments, and Partial Charges. *Journal of Chemical Theory and Computation*, *15*(6), 3678–3693. https://doi.org/10.1021/acs.jctc.9b00181

Wang, L.-P., & Song, C. (2016). Geometry optimization made simple with translation and rotation coordinates. *The Journal of Chemical Physics*, *144*(21). https://doi.org/10.1063/1.4952956

Wang, W., Wang, J., Dong, S., Liu, C., Italiani, P., Sun, S., Xu, J., Boraschi, D., Ma, S., & Qu, D. (2010). Immunomodulatory activity of andrographolide on macrophage activation and specific antibody response. *Acta Pharmacologica Sinica*, *31*(2), 191–201. https://doi.org/10.1038/aps.2009.205

Zarić, M. M., Radović, I. R., & Kijevčanin, M. L. (2020). Intermolecular interactions of cis-3-hexen-1-ol or 1-hexanol with n-hexane: Thermodynamic study, FT-IR analysis and quantum chemical calculations. *Journal of Molecular Liquids*, *303*, 112486. https://doi.org/10.1016/j.molliq.2020.112486

Zhang, J., Lu, H., Ruan, Y., Huang, S., Deng, S., Wang, Y., Li, Q., Zhao, Z., Feng, L., & Guo, W. (2024). Effects and Mechanisms of Andrographolide for COVID-19: A Network Pharmacology-Based and Experimentally Validated Study. *Natural Product Communications*, *19*(10). https://doi.org/10.1177/1934578X241288428

Zuhriyah, N., Fatkhurrohman, F., Aida, M., Apriliani, S., & Setiyono, E. (2025). In silico study of andrographolide bioactive compound from Andrographis paniculata as a potential anti-photoaging agent. *Biogenesis: Jurnal Ilmiah Biologi*, *12*(2), 16–27. https://doi.org/10.24252/bio.v12i2.57447